WAVES IN RANDOM AND COMPLEX MEDIA
https://doi.org/10.1080/17455030.2024.2341283

Taylor & Francis
Taylor & Francis Group

A probabilistic approach to modelling ultrasonic shear wave propagation in locally anisotropic heterogeneous media

Alistair S. Ferguson[a], Katherine M. M. Tant[a], Mohammud Foodun[a] and Anthony J. Mulholland[b]

[a]Department of Mathematics and Statistics, University of Strathclyde, Glasgow, UK; [b]Department of Engineering Mathematics, University of Bristol, Bristol, UK

ABSTRACT

This article considers the propagation of a high-frequency time harmonic, elastic wave in a spatially heterogeneous, randomly layered material. The material is locally anisotropic, and the material properties change from one layer to the next by a random rotation of the associated slowness surface in the plane of wave propagation. The layer thicknesses and this rotation follow a stochastic (Markovian) process. This situation is found in ultrasonic wave propagation in polycrystalline materials; for example, in the ultrasonic non-destructive testing of welds and additively manufactured metallic components. This work focuses on monochromatic shear waves propagating in a two-dimensional plane. Using the differences in length scales between the ultrasound wavelength, the mean layer size, and the wave propagation distance, a small parameter is identified in the stochastic differential equation that emerges. Its infinitesimal generator leads to a Fokker–Planck equation via limit theorems involving this small parameter. A weak form of the Fokker–Planck equation is derived and then solved via a finite element package. The numerical solution to the Fokker–Planck equation is used to compute statistical moments of the power transmission coefficient. Finally, a parametric study on the effect of the degree of anisotropy (asphericity of the slowness surface) of the material on the transmitted energy is performed.

ARTICLE HISTORY
Received 30 September 2023
Accepted 26 March 2024

KEYWORDS
Fokker–Planck; probabilistic; layered; anisotropic; ultrasound; elastic; moments

AMS SUBJECT CLASSIFICATIONS
35R60; 60H15; 65M60; 35Q86; 60F05

1. Introduction

This paper focuses on the propagation of ultrasound waves in elastic media which has a heterogeneous microstructure (that is, the material properties vary on a length scale commensurate with the wavelength, see Figure 1) and this microstructure varies randomly from one realization to another. This property is present in a plethora of engineering materials, and in particular welds and additively manufactured metals [1,2]. It is common practise when performing NDE (non-destructive evaluation) on an unknown material to assume homogeneous material properties. However, this is a physically unrealistic assumption in many materials of interest [3–5]. Wavelength-size grain-like structures exist in many industry relevant materials and waves propagating through such heterogeneous media

CONTACT Alistair S. Ferguson alistair@bosonmail.com

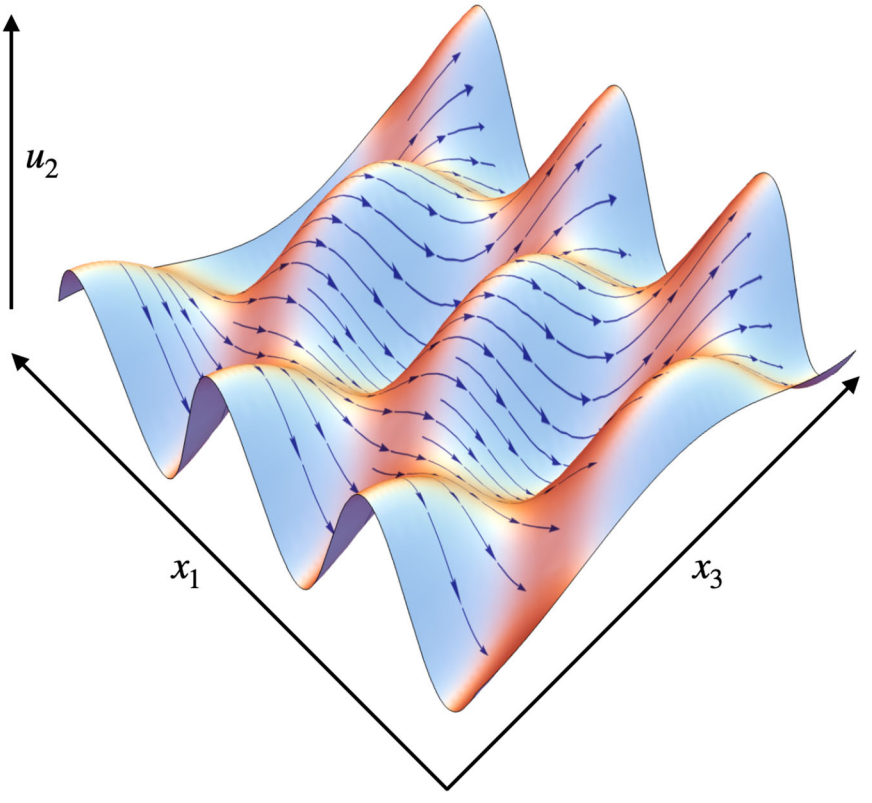

Figure 1. Elastic shear wavefront depiction moving in the (x_1, x_3) plane with displacement vector $\mathbf{u} = (0, u_2(x_1, x_3), 0)^T$. The arrows depict the orientation of the slowness surface associated with the underlying crystalline material.

experience scattering that converts the coherent input wave into small incoherent fluctuations which distort and attenuate the wave (studied extensively in [6] where the material is considered to be deterministic) which exits the material. There is interest within the non-destructive testing community to better understand ultrasonic wave propagation through such random media. There are many examples of components in which a heterogeneous microstructure exists and interacts with the propagating wave [7] to such an extent that the received wave has a significant incoherent component and bears little resemblance to the input waveform. This means that the medium cannot be characterized using homogenization. The received wave will vary from one sample/weld-site to the next and so it makes sense to describe the wave properties as a probability distribution and to use a probabilistic framework to model this phenomenon. Only via computationally prohibitive Monte Carlo simulations [8–10] can deterministic models [11] of wave propagation provide a similar characterization of wave propagation in such materials.

Additive Manufacturing (AM) is an emerging key technology for the manufacturing of high value and safety critical metallic components, such as those found in the aircraft engines, enabling automation in manufacturing, and tailored and bespoke customer designs. However, to achieve industry uptake, outstanding challenges associated with in situ quality control and inspection of the AM components need to be addressed [12]; the

full benefits of AM have yet to be realized due to the lack of inspection methods [13,14]. Laser-based ultrasound arrays offer a potential way forward due to the non-contact and broadband nature of such sensors [15]. They could be used to tomographically reconstruct the internal grain structure of these components and thus allow the component quality assurance to be performed. It is necessary however for the frequency of the input wave to be carefully chosen to ensure that the wave undergoes a complex interaction (multiple scattering events) with the material microstructure. In this way the time domain waveforms that emerge have encoded within them details of the inner structure of the component and importantly a codification of the presence of flaws. As each component has a distinct and random microstructure then, in order to reconstruct this microstructure, each component must give rise to a distinct transmitted wave. In other words we need to operate in a regime where we maximize the sensitivity of the wave to the microstructure and hence in a regime where the variation in the statistics of the received from one component to another is maximized. The model created in this paper could be used to optimize the choice of the frequency of the input ultrasound wave by maximizing the variation in the transmission coefficient in a population of components with a stochastic microstructure. Hence this paper can contribute to the current efforts to create a viable quality assurance inspection method for AM metallic components.

This paper considers a layered random media ($x_3 \in [0, L]$) embedded between two homogeneous half-spaces ($x_3 \in (-\infty, 0) \cup (L, \infty)$). A time harmonic (monochromatic) source plane wave is located in the left-hand half-space $x_3 \in (-\infty, 0)$. The media consists of a single material with a constant density ρ but a spatially dependent elastic tensor c_{ijkl}; this is a common situation in NDE relevant materials such as polycrystalline welds or additively manufactured metals. The layer by layer generation of the material in the x_3 direction, and its solidification as it cools, leads to a layered structure of grains [16] where the temperature gradients lead to random variations in crystal orientation in each layer (see Figure 1) and a distribution of layer sizes which follow a Poisson distribution (see the experimental results in [17]). Guided by physical observations, the spatial variations in the material properties primarily depend on the depth x_3 into the material. This paper will consider a monochromatic plane wave traveling in the (x_1, x_3) plane whose displacement is in the x_2 direction only, as described by the displacement vector $\mathbf{u} = (0, u_2(x_1, x_3), 0)$. The plane wave propagates in the x_3 direction and the wave particles vibrate in the x_2 direction perpendicular to the (x_1, x_3) plane with the amplitude of oscillation varying across this plane. A key parameter which will emerge is $\nu = \kappa_1/\kappa_3$, the ratio of wavenumbers in the x_1 and x_3 directions, which captures the degree of anisotropy of the elastic medium.

The form of the elastic tensor stems from [1] where the authors investigated the propagation of elastic shear waves in a class of anisotropic materials motivated by non-destructive testing and geophysics problems. The deterministic model outlined in [1] describes elastic waves propagating in heterogeneous locally anisotropic media. In particular, the material is transversely isotropic, the zonal axis of symmetry lies in the (x_1, x_3) plane, and all cross-sections perpendicular to the x_2 axis are identical. θ is defined to be the angle that the zonal axis makes with the x_3 axis at any particular position in the material. Hence, the material is rotated about the x_2 axis by different amounts depending on the particular location in the (x_1, x_3) plane. This rotation of the stiffness tensor can be interpreted as a rotation of an associated slowness surface (or slowness curve in this planar case) where the rotation $\theta(x_3)$ is a piecewise-constant function.

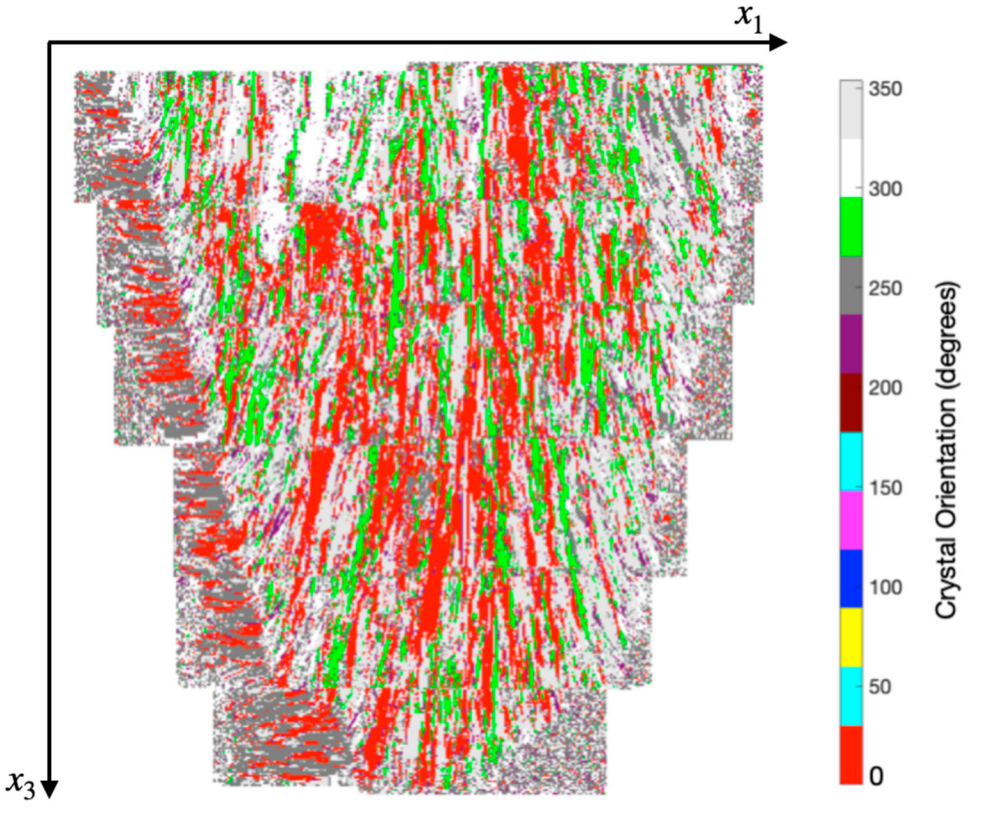

Figure 2. Fanned grain structure of a heterogeneous weld structure. This image shows a simplified representation of the material properties as measured destructively using electron backscatter diffraction (EBSD) which shows clusters of grains of wavelength size. The colors correspond to different crystal orientations (θ) inside the weld. Image generated from data obtained in [42,43].

This paper adopts this formulation of the constitutive law for a specific material (austenitic steel) and the associated rotation of the slowness surface θ about the x_2 axis, which is linked to the directionality of the cooling process [18]. As the metal cools in the weld, the crystalline structures elongate and align with the direction of the thermal gradients (see Figure 2). In this paper however, a stochastic spatial variation of the slowness surface is assumed to capture the random fluctuations in the crystalline alignment in the material.

The deterministic modeling of ultrasound waves in layered, locally anisotropic media has been studied for many years in applications such as geophysics [19,20] and non-destructive testing [21]. The incident traveling wave enters the layered media at a given angle and the change in wave mode between layers is given by the Christoffel equation to create upward and downward traveling waves [22] where mode conversion is accounted for. A transfer matrix between each layer is calculated which relates the displacements and stresses in adjacent layers through the continuity of stress and displacement at each layer interface [23]. In this recursive manner a transfer matrix for the entire structure can be determined. Based on this recursive principal there are a number of closely related methods such

as the stiffness matrix approach [24] (where the stresses are first linked to the displacements in a given layer via a stiffness matrix), the mixed variable method [25] (which links the displacement vector at one layer interface to the stress vector at the other layer interface), and the surface impedance matrix approach [26] (where the velocity field is linked to the stress field at each interface). The approach can be developed to utilize analytical solutions obtained via a Fourier spectral method where each layer has infinite lateral extent [27]. In the case where the layer thickness is much smaller than the wavelength then it is possible to use homogenization to derive an equivalent homogeneous medium [28]. This can be used to develop ultrasonic array imaging algorithms that can correct for the layered structure [29]. In the context of soil dynamics [30] a Green's function approach has been used to describe the displacement and stress at any point in layered, locally anisotropic media [31]. By applying a Fourier-Bessel transform to convert the elastodynamic equations of motion into a wavenumber domain, the precise integration method (PIM) is then used to obtain the Green's function and the inverse Fourier-Bessel transform applied. The resulting integral equation is solved numerically. This approach can address some of the instabilities that can arise in recursive methods such as the transfer matrix approach. Alternatively a Fourier transform approach can be deployed [32]. Legendre polynomial methods have been used when the layered structure forms a plate and the study then looks at coupled Lamb waves [33]. Modeling of ultrasonic wave propagation in anisotropic media, with embedded scatterers, can be conducted using numerical integration of the time domain elastodynamic equations via finite elements [34]. However, to improve on the computational efficiency from a scattering object within a multi-layered, locally anisotropic, elastic media then Gaussian beams (to model the ultrasonic transducer source wave) and a localized equivalent homogenized media surrounding the scatterer (to obtain an analytic expression for the angular scattering coefficient), combined with a recursive stiffness matrix method has been developed [35]. As the application is focused on manufactured composites then each layer has the same thickness and this thickness is commensurate with the wavelength of the incident wave. The transfer matrix approach can include the effects of random fluctuations in the layer sizes using random matrices, coupled with Furstenberg's theorem and Monte Carlo simulation, to comment on the frequency dependency of the mean transmission coefficient [36]. It can also be extended to include piezoelectric layers [37] and, via a plane wave expansion approach, fractal piezoelectric structures in ultrasonic array design [38]. Furthermore, elastic wave scattering at grain boundaries has been investigated in order to determine material microstructure properties [39] by studying the grain width distribution; many metals have a log normal distribution of grain widths which will affect wave transmission.

One of the deficiencies of a deterministic approach is that one needs to perform computationally expensive Monte Carlo simulations in order to establish the statistical variance in transmitted waves across a population of components with distinct interior microstructures. This paper pursues the alternative approach of adopting a probabilistic framework that automatically produces such information. An appropriate framework that was initially developed for high frequency waves in randomly layered fluids [40] has very recently been extended to solids [6]. Propagation of monochromatic shear waves in a randomly layered transversely isotropic elastic media was studied where the wave vibrates perpendicular to the direction of wave propagation (x_3) and the wave amplitude was only dependent on x_3. This paper extends this work to consider the AM inspection relevant case where the

displacement also depends on the lateral direction (x_1). In addition, the rotation of the slowness surface was around the x_3 axis in [6,41]; the associated slowness surface led to a set of wave-mode equations which had a conjugate symmetry which resulted in a simplified set of governing equations. In this paper however we study the AM relevant case where the crystal rotation is in the plane of propagation (x_1, x_2). These changes lead to a richer and more complex model as illustrated by the intractable Fokker–Planck equation which emerges. This paper considers the case where the material consists of a series of layers in the x_3 direction with a random rotation θ_j in the jth layer of the material (see Figure 1).

Section 2 introduces the governing elastic wave equation, the wave-mode equations and the physical geometry of the problem. Section 3.1 introduces a stochastic (Markovian) process to model the variations in the local orientation of the slowness surface. In the weakly heterogeneous scaling regime a small parameter emerges in the governing random wave-mode evolution equations. A diffusion approximation is then used to derive stochastic differential equations in order to study the probability distribution of the transmitted energy. A Fokker–Planck equation is derived for the probability density function for the transmitted energy which then is solved numerically via a finite element solver using Python [44]. Section 4 contains a discussion of the power transmission coefficient and a parametric study on an austenitic steel weld.

2. Governing elastic wave equations

In this Section we will derive the equations of motion of a horizontally polarized shear wave in a layered locally anisotropic elastic medium. The elastodynamic equation of wave motion is [1]

$$\rho\, u_{j,tt} = \tau_{jk,k}, \tag{1}$$

where ρ is the density of the medium, u is the displacement, and τ is the stress. The general stress-strain law is of the form

$$\tau_{ij} = c_{ijkl}(\theta(x_3))e_{kl}, \tag{2}$$

with

$$e_{kl} = \frac{1}{2}\,(u_{k,l} + u_{l,k}), \tag{3}$$

where c_{ijkl} is the stiffness tensor, and e_{kl} is the direct strain. Define

$$c_{pqrs} = a_{ip}\, a_{jq}\, a_{kr}\, a_{ls}\, \bar{\bar{c}}_{ijkl}, \tag{4}$$

where a_{ij} describes a rotation θ about the x_2 axis, where θ is dependent on x_3 and the locally transversely isotropic matrix $\bar{\bar{c}}_{ijkl}$ is of the form

$$\bar{\bar{c}}_{ijkl} = \bar{\bar{c}}_{mn} = \begin{bmatrix} \bar{\bar{c}}_{11} & \bar{\bar{c}}_{12} & \bar{\bar{c}}_{13} & 0 & 0 & 0 \\ \bar{\bar{c}}_{12} & \bar{\bar{c}}_{11} & \bar{\bar{c}}_{13} & 0 & 0 & 0 \\ \bar{\bar{c}}_{13} & \bar{\bar{c}}_{13} & \bar{\bar{c}}_{33} & 0 & 0 & 0 \\ 0 & 0 & 0 & \bar{\bar{c}}_{44} & 0 & 0 \\ 0 & 0 & 0 & 0 & \bar{\bar{c}}_{44} & 0 \\ 0 & 0 & 0 & 0 & 0 & \bar{\bar{c}}_{66} \end{bmatrix}. \tag{5}$$

Austenitic steel welds are a commonly used material in the engineering world, exhibiting material properties that align with Equation (5). Considering a horizontally polarized shear wave, u_j can be expressed as

$$u_j = (0, u_2(x_1, x_3), 0). \tag{6}$$

Therefore, Equations (2) and (3) give

$$\tau_{21} = c_{66}(x_3)u_{2,1} + c_{46}(x_3)u_{2,3}, \tag{7}$$

$$\tau_{23} = c_{46}(x_3)u_{2,1} + c_{44}(x_3)u_{2,3}, \tag{8}$$

where (noting that $c_{64}(x_3) = c_{46}(x_3)$)

$$c_{66}(x_3) = \cos^2\theta(x_3)\bar{\bar{c}}_{66} + \sin^2\theta(x_3)\bar{\bar{c}}_{44} \tag{9}$$

$$c_{64}(x_3) = -\cos\theta(x_3)\sin\theta(x_3)\bar{\bar{c}}_{66} + \sin\theta(x_3)\cos\theta(x_3)\bar{\bar{c}}_{44} \tag{10}$$

$$c_{44}(x_3) = \sin^2\theta(x_3)\bar{\bar{c}}_{66} + \cos^2\theta(x_3)\bar{\bar{c}}_{44}. \tag{11}$$

Defining the velocity $\xi = u_{2,t}$, then Equation (1) becomes

$$\rho\,\xi_{,t} = \tau_{21,1} + \tau_{23,3}, \tag{12}$$

and differentiating (7) and (8) with respect to t gives

$$\tau_{21,t} = c_{66}(x_3)\,\xi_{,1} + c_{46}(x_3)\,\xi_{,3}, \tag{13}$$

$$\tau_{23,t} = c_{46}(x_3)\,\xi_{,1} + c_{44}(x_3)\,\xi_{,3}. \tag{14}$$

Define the Fourier transforms with respect to time as

$$\check{\xi}(\omega, \underline{x}) = \int \xi_2(t, x_1, x_3)\,\mathrm{e}^{i\omega t}\,\mathrm{d}t, \tag{15}$$

and with respect to x_1 as

$$\hat{\check{\xi}}(\omega, \kappa_1, x_3) = \int \check{\xi}(\omega, x_1, x_3)\,\mathrm{e}^{i\kappa_1 x_1}\,\mathrm{d}x_1, \tag{16}$$

where κ_1 is the wavenumber in the x_1 direction. Applying these transformations to Equations (12), (13) and (14) leads to

$$\hat{\tau}_{23,3} = \psi(\omega, \kappa_1, x_3)\hat{\check{\xi}} + \varsigma(\kappa_1, x_3)\hat{\tau}_{23}, \tag{17}$$

where $\psi(\omega, \kappa_1, x_3) = -i\omega(\rho - \kappa_1^2 c_{66}(x_3)/\omega^2 + \kappa_1^2 c_{64}(x_3)^2/(\omega^2 c_{44}(x_3))) = -i\omega\hat{\psi}(\omega, \kappa_1, x_3)$ and $\varsigma(\kappa_1, x_3) = i\kappa_1 c_{64}(x_3)/c_{44}(x_3) = i\hat{\varsigma}(\kappa_1, x_3)$ and so

$$\hat{\check{\xi}}_{,3} = \varsigma(\kappa_1, x_3)\hat{\check{\xi}} - \eta(\omega, x_3)\hat{\tau}_{23}, \tag{18}$$

where $\eta(\omega, x_3) = i\omega/c_{44}(x_3) = i\hat{\eta}(\omega, x_3)$, with $\hat{\check{\xi}}(\omega, \kappa_1, x_3)$, $\hat{\tau}(\omega, \kappa_1, x_3) : \mathbb{R}^3 \to \mathbb{R}$ and the boundary conditions are the radiation conditions whereby $\hat{\check{\xi}} \to 0$ as $x_3 \to \pm\infty$ and $\hat{\tau} \to 0$ as $x_3 \to \pm\infty$, and a wave is initiated by imposing an initial stress $\hat{\tau}_0$ and velocity $\hat{\check{\xi}}_0$ at $x_3 = 0$. Equations (17) and (18) form the basis of the system of evolution equations that will be derived in Section 3.

3. Probability density function for the power transmission coefficient

The aim of this Section is to derive a Fokker–Planck equation that describes the evolution of a probability density function for the power transmission coefficient as the wavefront moves through this randomly layered structure. In Section 3.1 we introduce Taylor expansions in the slowness surface angle (θ) to make analytical headway. Within Section 3.2 we non-dimensionalize the problem and choose appropriate length scales to study the weakly heterogeneous regime; this allows us to obtain a set of stress-strain evolution equations. In Section 3.3 we apply a diffusion approximation theorem to obtain a system of evolution equations that describe the behavior of the wave via the propagator functions (from Equation (66)).

3.1. Randomly layered anisotropic medium

For simplicity, assume that the local orientation of the slowness surface $\theta(x_3)$ varies randomly over the interval $x_3 \in [0, L]$ according to the additive noise formulation

$$\theta(x_3) = \bar{\theta} + \sigma m(x_3/l), \quad x_3 \in [0, L], \tag{19}$$

where $\bar{\theta} \sim 1$ is the mean orientation, $m(x_3/l)$ is a stationary stochastic process (an ergodic Markov process on a compact state space) with mean zero and unit variance, and $0 < \sigma \ll 1$ is a small parameter. From Equation (4) the stress tensor components can be rewritten

$$c_{66} = \sin^2(\bar{\theta} + \sigma m(x_3/l))F + \cos^2(\bar{\theta} + \sigma m(x_3/l))N, \tag{20}$$

$$c_{44} = \sin^2(\bar{\theta} + \sigma m(x_3/l))N + \cos^2(\bar{\theta} + \sigma m(x_3/l))F, \tag{21}$$

and

$$c_{64} = \sin(\bar{\theta} + \sigma m(x_3/l))\cos(\bar{\theta} + \sigma m(x_3/l))(F - N), \tag{22}$$

where $N = \bar{\bar{c}}_{66}$ and $F = \bar{\bar{c}}_{44}$ when $\bar{\theta} = 0$. Taking a Taylor series in σ gives

$$c_{66} = \bar{c}_{66}(1 + \sigma_{66} m(x_3/l)), \tag{23}$$

where $\bar{c}_{66} = N\cos^2\bar{\theta} + F\sin^2\bar{\theta}$, and $\sigma_{66} = \sigma \sin 2\bar{\theta}(F - N)/\bar{c}_{66}$. Next

$$c_{44} = \bar{c}_{44}(1 + \sigma_{44} m(x_3/l)), \tag{24}$$

where $\bar{c}_{44} = N\sin^2\bar{\theta} + F\cos^2\bar{\theta}$ and $\sigma_{44} = \sigma \sin 2\bar{\theta}(N - F)/\bar{c}_{44}$, and

$$c_{64}(x_3) = \bar{c}_{64}(1 + \sigma_{64} m(x_3/l)), \tag{25}$$

where $\bar{c}_{64} = (F - N)\sin 2\bar{\theta}/2$ and $\sigma_{64} = 2\sigma \cot 2\bar{\theta}$. From Equation (17) ς becomes

$$\varsigma(\kappa_1, x_3) = \bar{\hat{c}}_{64}(\kappa_1)(1 + \hat{\sigma}_{64} m(x_3/l)), \tag{26}$$

where

$$\bar{\hat{c}}_{64} = \frac{i\kappa_1 \bar{c}_{64}}{\bar{c}_{44}}, \tag{27}$$

and $\hat{\sigma}_{64} = \sigma_{64} - \sigma_{44} = \sigma\,(2\cot 2\bar{\theta} + \sin 2\bar{\theta}(F-N)/\bar{c}_{44}) = \sigma\,\Gamma_\alpha$ and $\Gamma_\alpha = 2\cot 2\bar{\theta} + \sin 2\bar{\theta}(F-N)/\bar{c}_{44}$. From Equation (18) to $\mathcal{O}(\sigma)$

$$\eta(\omega, x_3) = \bar{\hat{c}}_{44}(\omega)(1 + \hat{\sigma}_{44}(\omega) m(x_3/l)), \tag{28}$$

where

$$\bar{\hat{c}}_{44} = \frac{i\omega}{\bar{c}_{44}}, \tag{29}$$

and $\hat{\sigma}_{44} = -\sigma_{44} = \sigma\,\Gamma_\beta$ and $\Gamma_\beta = \sin 2\bar{\theta}(F-N)/\bar{c}_{44}$. From Equation (17) to $\mathcal{O}(\sigma)$

$$\psi(\omega, \kappa_1, x_3) = \bar{\hat{\psi}}(\omega, \kappa_1)(1 + \hat{\sigma}_\psi(\omega, \kappa_1) m(x_3/l)), \tag{30}$$

where

$$\bar{\hat{\psi}}(\omega, \kappa_1) = \frac{-i(\bar{c}_{64}^2 - \bar{c}_{66}\bar{c}_{44})\kappa_1^2 - i\rho\omega^2\bar{c}_{44}}{\bar{c}_{44}\omega}, \tag{31}$$

$\hat{\sigma}_\psi(\omega, \kappa_1) = \sigma\,\Gamma_\gamma$ and

$$\Gamma_\gamma = \frac{\kappa_1^2(\bar{c}_{64}^2(4\cot 2\bar{\theta} + \sin 2\bar{\theta}(F-N)/\bar{c}_{44}) - \bar{c}_{44}\sin 2\bar{\theta}(F-N))}{(\bar{c}_{64}^2 - \bar{c}_{44}\bar{c}_{66})\kappa_1^2 + \rho\omega^2\bar{c}_{44}}. \tag{32}$$

3.2. Weakly heterogeneous scaling regime

In this section, the governing equations will be non-dimensionalized by introducing appropriate length scales. The wave modes, both left- and right-going, will be analyzed and the propagator matrix will be derived. This will enable the transformation of the problem from a boundary value problem to an initial value problem.

Denote the wavelength by λ_3, the wave propagation distance by L_3 and the mean layer size in the media by l. In what follows $L_3 \gg \lambda_3 \sim l$ and the amplitude of the fluctuations in the spatially varying material properties satisfies $0 < \sigma \ll 1$; this is the so-called weakly heterogeneous regime [40]. This setting causes fluctuations to build up behind the transmitted wave, producing an incoherent coda wave containing the bulk of the wave energy. Now non-dimensionalize the governing equations via the transformations

$$\tilde{x}_3 = \frac{x_3}{L_3}, \quad \tilde{\omega} = \frac{L_3\,\omega}{c_3}, \text{ and } \tilde{\kappa}_1 = \kappa_1 L_3, \tag{33}$$

where c_3 is the mean shear wave speed in the x_3 direction. $\tilde{x}_3$ can be interpreted as a ratio of distances in the propagation direction, $\tilde{\omega}$ as a ratio of the propagation distance to the typical wavelength in the propagation direction and $\tilde{\kappa}_1$ as a ratio of propagation distance per wavelength in the x_1 direction. Define two dimensionless parameters ε and ϖ to capture

the length scale differences via

$$0 < \epsilon \ll 1, \quad \frac{L_3}{l} = \frac{1}{\varepsilon^2}, \quad \tilde{\omega} = \frac{\omega L_3}{c_3} = \frac{\varpi}{\varepsilon}. \tag{34}$$

The ratio ϖ/ε is the propagation distance measured in units of wavelength. These relations can be combined to write

$$\varepsilon = \sqrt{\frac{l}{L_3}}, \quad \text{and} \quad \varpi = \frac{\omega}{c_3}\sqrt{lL_3} = \varepsilon\tilde{\omega}. \tag{35}$$

The non-dimensional velocity and stress fields take the form

$$\tilde{\xi}(\tilde{\omega}, \tilde{\kappa_1}, \tilde{x_3}) = \frac{1}{c_3}\hat{\xi}\left(\frac{c_3\tilde{\omega}}{L_3}, \frac{\omega_3\tilde{\kappa_1}}{c_3}, L_3\tilde{x_3}\right), \quad \tilde{\tau}(\tilde{\omega}, \tilde{\kappa_1}, \tilde{x_3}) = \frac{1}{\rho c_3^2}\hat{\tau}\left(\frac{c_3\tilde{\omega}}{L_3}, \frac{\omega_3\tilde{\kappa_1}}{c_3}, L_3\tilde{x_3}\right). \tag{36}$$

The non-dimensional stress and velocity equations are then (from Equations (17), (18), (28) and (30))

$$\tilde{\xi}_{,3} = L_3\bar{\tilde{c}}_{64}\left(1 + \hat{\sigma}_{64}m\left(\frac{\tilde{x}_3}{\varepsilon^2}\right)\right)\tilde{\xi} - \rho c_3 L_3\bar{\tilde{c}}_{44}\left(1 + \hat{\sigma}_{44}m\left(\frac{\tilde{x}_3}{\varepsilon^2}\right)\right)\tilde{\tau}, \tag{37}$$

$$\tilde{\tau}_{,3} = \frac{L_3}{\rho c_3}\bar{\tilde{\psi}}\left(1 + \hat{\sigma}_{\psi}m\left(\frac{\tilde{x}_3}{\varepsilon^2}\right)\right)\tilde{\xi} + L_3\bar{\tilde{c}}_{64}\left(1 + \hat{\sigma}_{64}m\left(\frac{\tilde{x}_3}{\varepsilon^2}\right)\right)\tilde{\tau}. \tag{38}$$

These equations have three non-dimensional lumped parameters. From Equation (27)

$$L_3\bar{\tilde{c}}_{64} = i\frac{\kappa_1 L_3\bar{c}_{64}}{\bar{c}_{44}} = i\tilde{\kappa}_1\frac{\tilde{c}_{64}}{\tilde{c}_{44}}, \tag{39}$$

where $\tilde{c}_{64} = \bar{c}_{64}/(\rho c_3^2)$ and $\tilde{c}_{44} = \bar{c}_{44}/(\rho c_3^2)$. Also, from Equations (29) and (33)

$$\rho c_3 L_3\bar{\tilde{c}}_{44} = \rho c_3 L_3\frac{i\omega}{\bar{c}_{44}} = i\frac{\rho c_3^2}{\bar{c}_{44}}\frac{\omega L_3}{c_3} = \frac{i\tilde{\omega}}{\tilde{c}_{44}}. \tag{40}$$

From Equation (31)

$$\frac{L_3}{\rho c_3}\bar{\tilde{\psi}} = -i\tilde{\omega}\left(1 + \frac{\tilde{\kappa}_1^2}{\tilde{\omega}^2}\left(\frac{\tilde{c}_{64}^2}{\tilde{c}_{44}} - \tilde{c}_{66}\right)\right), \tag{41}$$

where $\tilde{c}_{66} = \bar{c}_{66}/(\rho c_3^2)$. Equations (37) and (38) then become

$$\tilde{\xi}_{,3} = i\tilde{\kappa}_1\frac{\tilde{c}_{64}}{\tilde{c}_{44}}\left(1 + \hat{\sigma}_{64}m\left(\frac{\tilde{x}_3}{\varepsilon^2}\right)\right)\tilde{\xi} + i\tilde{\omega}\left(\frac{-1}{\tilde{c}_{44}}\right)\left(1 + \hat{\sigma}_{44}m\left(\frac{\tilde{x}_3}{\varepsilon^2}\right)\right)\tilde{\tau}, \tag{42}$$

$$\tilde{\tau}_{,3} = -i\tilde{\omega}\left(1 + \frac{\tilde{\kappa}_1^2}{\tilde{\omega}^2}\left(\frac{\tilde{c}_{64}^2}{\tilde{c}_{44}} - \tilde{c}_{66}\right)\right)\left(1 + \hat{\sigma}_{\psi}m\left(\frac{L_3}{l}\tilde{x}_3\right)\right)\tilde{\xi} + i\tilde{\kappa}_1\frac{\tilde{c}_{64}}{\tilde{c}_{44}}\left(1 + \hat{\sigma}_{64}m\left(\frac{\tilde{x}_3}{\varepsilon^2}\right)\right)\tilde{\tau}, \tag{43}$$

where $\tilde{c}_{44}, \tilde{c}_{64}, \tilde{c}_{66} \sim 1$. The prefactor in Equation (43) is

$$\frac{\tilde{\kappa}_1}{\tilde{\omega}} = \frac{\kappa_1 L_3}{(L_3\omega/c_3)} = \frac{\kappa_1}{\kappa_3} = \nu, \text{ say,} \tag{44}$$

where κ_3 is the mean wavenumber in the x_3 direction, and hence ν is the ratio of wavenumbers in the (x_1, x_3) directions. For a monochromatic wave the ratio of wavenumbers is equal

to the ratio of slowness (the inverse of the phase velocity) values which in turn (for constant density materials) is the degree of anisotropy of the medium as governed by the stiffness tensor Equation (5). As the crystal orientation θ changes, the phase velocities in the x_1 and x_3 direction change and hence, the wavenumbers in these directions change commensurately. Using Equations (42), (43), (34) and (44) gives

$$\frac{\partial}{\partial \tilde{x}_3}\begin{bmatrix}\tilde{\xi}(\tilde{\omega},\tilde{\kappa_1},\tilde{x_3})\\ \tilde{\tau}(\tilde{\omega},\tilde{\kappa_1},\tilde{x_3})\end{bmatrix} = i\frac{\varpi}{\varepsilon}\begin{bmatrix}\tilde{\alpha}(1+\sigma\Gamma_\alpha m(\tilde{x}_3/\varepsilon^2)) & \tilde{\beta}(1+\sigma\Gamma_\beta m(\tilde{x}_3/\varepsilon^2))\\ \tilde{\gamma}(1+\sigma\Gamma_\gamma m(\tilde{x}_3/\varepsilon^2)) & \tilde{\alpha}(1+\sigma\Gamma_\alpha m(\tilde{x}_3/\varepsilon^2))\end{bmatrix}\begin{bmatrix}\tilde{\xi}(\tilde{\omega},\tilde{\kappa_1},\tilde{x_3})\\ \tilde{\tau}(\tilde{\omega},\tilde{\kappa_1},\tilde{x_3})\end{bmatrix}, \tag{45}$$

where the new non-dimensional variables are defined as

$$\tilde{\alpha} = \nu\frac{\tilde{c}_{64}}{\tilde{c}_{44}}, \tag{46}$$

$$\tilde{\beta} = -\frac{1}{\tilde{c}_{44}}, \tag{47}$$

$$\tilde{\gamma} = -\left(1+\nu^2\left(\frac{\tilde{c}_{64}^2}{\tilde{c}_{44}}-\tilde{c}_{66}\right)\right), \tag{48}$$

where Equation (32) now becomes

$$\Gamma_\gamma = \frac{\nu^2(\sin 2\bar{\theta}(F-N)(\bar{c}_{44}^2-\bar{c}_{64}^2)-4\bar{c}_{44}\bar{c}_{64}^2\cot 2\bar{\theta})}{\bar{c}_{44}(\nu^2(\bar{c}_{66}\bar{c}_{44}-\bar{c}_{64}^2)-\bar{c}_{44}\rho c_3^2)}, \tag{49}$$

and where $\tilde{\alpha}$, $\tilde{\beta}$ and $\tilde{\gamma}$ are $\mathcal{O}(1)$. Temporarily setting $m(x_3/\varepsilon^2)=0$ in Equation (45) gives

$$\frac{\partial}{\partial x_3}\begin{bmatrix}\tilde{\xi}\\ \tilde{\tau}\end{bmatrix} = i\frac{\varpi}{\varepsilon}\begin{bmatrix}\tilde{\alpha} & \tilde{\beta}\\ \tilde{\gamma} & \tilde{\alpha}\end{bmatrix}\begin{bmatrix}\tilde{\xi}\\ \tilde{\tau}\end{bmatrix} = M\begin{bmatrix}\tilde{\xi}\\ \tilde{\tau}\end{bmatrix}. \tag{50}$$

The eigenvalues of M are $\Lambda^{\pm} = i\omega/\varepsilon(\tilde{\alpha}\pm\sqrt{\tilde{\beta}\tilde{\gamma}})$ and the eigenvectors are $[\sqrt{\tilde{\beta}\tilde{\gamma}},\ \tilde{\gamma}]^T$ and $[-\sqrt{\tilde{\beta}\tilde{\gamma}},\ \tilde{\gamma}]^T$. Let

$$\phi = \sqrt{\beta\gamma} = \sqrt{\frac{1+\nu^2\left(\frac{\tilde{c}_{64}^2}{\tilde{c}_{44}}-\tilde{c}_{66}\right)}{\tilde{c}_{44}}}. \tag{51}$$

To ease notation, now drop the bars on the prefactors. Now consider the following ansatz for the generated right-moving modes $\hat{a}^\varepsilon(\omega,\kappa_1,x_3)$ and left-moving modes $\hat{b}^\varepsilon(\omega,\kappa_1,x_3)$

$$\begin{bmatrix}\hat{\xi}(\omega,\kappa_1,x_3)\\ \hat{\tau}(\omega,\kappa_1,x_3)\end{bmatrix} = \begin{bmatrix}\sqrt{\zeta/\gamma} & -\sqrt{\zeta/\gamma}\\ \sqrt{\gamma/\zeta} & \sqrt{\gamma/\zeta}\end{bmatrix}\begin{bmatrix}\hat{b}^\varepsilon(\omega,\kappa_1,x_3)\\ \hat{a}^\varepsilon(\omega,\kappa_1,x_3)\end{bmatrix}, \tag{52}$$

where $\zeta = \sqrt{\alpha\gamma}$ and

$$\hat{a}^\varepsilon(\omega,\kappa_1,x_3) = \hat{a}^\varepsilon(\omega,\kappa_1,x_3)\,\mathrm{e}^{\Lambda^{(-)}x_3}, \tag{53}$$

$$\hat{b}^\varepsilon(\omega,\kappa_1,x_3) = \hat{b}^\varepsilon(\omega,\kappa_1,x_3)\,\mathrm{e}^{\Lambda^{(+)}x_3}. \tag{54}$$

This produces a new system whose coefficients are zero centered random variables

$$\hat{a}^{\varepsilon} = \frac{1}{2}\left(\sqrt{\zeta/\gamma}\,\hat{\tau} - \sqrt{\gamma/\zeta}\,\hat{\xi}\right)\mathrm{e}^{-\Lambda^{(-)}x_3}, \tag{55}$$

$$\hat{b}^{\varepsilon} = \frac{1}{2}\left(\sqrt{\zeta/\gamma}\,\hat{\tau} + \sqrt{\gamma/\zeta}\,\hat{\xi}\right)\mathrm{e}^{-\Lambda^{(+)}x_3}. \tag{56}$$

Taking partial derivatives in x_3 gives

$$\frac{\partial \hat{a}^{\varepsilon}}{\partial x_3} = \frac{i\varpi}{2\varepsilon}\left(\Delta_1(x_3/\varepsilon^2)\hat{a}^{\varepsilon} + \Delta_2(x_3/\varepsilon^2)\hat{b}^{\varepsilon}\right), \tag{57}$$

and

$$\frac{\partial \hat{b}^{\varepsilon}}{\partial x_3} = \frac{i\varpi}{2\varepsilon}\left(\Delta_3(x_3/\varepsilon^2)\hat{a}^{\varepsilon} + \Delta_4(x_3/\varepsilon^2)\hat{b}^{\varepsilon}\right), \tag{58}$$

where $\Delta_1 = \sigma m(x_3/\varepsilon^2)\delta_1$, $\Delta_2 = \sigma m(x_3/\varepsilon^2)\delta_2\,\mathrm{e}^{2i\varpi\phi x_3/\varepsilon}$, $\Delta_3 = -\sigma m(x_3/\varepsilon^2)\delta_2\,\mathrm{e}^{-2i\varpi\phi x_3/\varepsilon}$ and $\Delta_4 = \sigma m(x_3/\varepsilon^2)\delta_4$. Also, $\delta_1 = 2\alpha\Gamma_\alpha - \phi(\Gamma_\beta + \Gamma_\gamma)$, $\delta_2 = \phi(\Gamma_\gamma - \Gamma_\beta)$ and $\delta_4 = 2\alpha\Gamma_\alpha + \phi(\Gamma_\gamma + \Gamma_\beta)$. Note here that α, β and γ are given by Equations (46), (47) and (48) and so are independent of x_3. The wave-mode amplitude evolution equations are therefore

$$\frac{\mathrm{d}}{\mathrm{d}x_3}\begin{bmatrix}\hat{a}^{\varepsilon}\\ \hat{b}^{\varepsilon}\end{bmatrix} = i\frac{\varpi\sigma}{2\varepsilon}m\left(\frac{x_3}{\varepsilon^2}\right)\begin{bmatrix}\delta_1 & \delta_2\,\mathrm{e}^{i2i\varpi\phi x_3/\varepsilon}\\ -\delta_2\,\mathrm{e}^{-i2i\varpi\phi x_3/\varepsilon} & \delta_4\end{bmatrix}\begin{bmatrix}\hat{a}^{\varepsilon}\\ \hat{b}^{\varepsilon}\end{bmatrix}. \tag{59}$$

Here $L_3 \gg \lambda_3$ and so from Equations (33) and (34)

$$1 \ll \frac{L_3}{\lambda_3} = \frac{\omega L_3}{2\pi c_3} = \frac{\tilde{\omega}}{2\pi} = \frac{\varpi}{2\pi\varepsilon}. \tag{60}$$

Here $\lambda_3 \sim l$ and so from Equation (35)

$$1 \sim \frac{l}{\lambda_3} = \frac{\omega l}{2\pi c_3} = \frac{\omega L_3}{2\pi c_3}\frac{l}{L_3} = \frac{\varpi}{2\pi\varepsilon}\varepsilon^2. \tag{61}$$

Hence, Equation (61) implies (with $0 < \varepsilon \ll 1$) that

$$\varpi \sim \frac{1}{\varepsilon}, \tag{62}$$

and so Equation (60) holds. Since $0 < \sigma \ll 1$ then set $\sigma = \varepsilon$. This gives the evolution Equation (59) in the form

$$\frac{\mathrm{d}}{\mathrm{d}x_3}\begin{bmatrix}\hat{a}^{\varepsilon}\\ \hat{b}^{\varepsilon}\end{bmatrix} = \frac{1}{\varepsilon}\mathbf{H}^{\varepsilon}\left(\frac{x_3}{\varepsilon^2}, m\left(\frac{x_3}{\varepsilon^2}\right)\right)\begin{bmatrix}\hat{a}^{\varepsilon}\\ \hat{b}^{\varepsilon}\end{bmatrix}, \tag{63}$$

where

$$\mathbf{H}^{\varepsilon}\left(\frac{x_3}{\varepsilon^2}, m\left(\frac{x_3}{\varepsilon^2}\right)\right) = \frac{i}{2}m(x_3/\varepsilon^2)\begin{bmatrix}\delta_1 & \delta_2\,\mathrm{e}^{2i\phi x_3/\varepsilon^2}\\ -\delta_2\,\mathrm{e}^{-2i\phi x_3/\varepsilon^2} & \delta_4\end{bmatrix}, \tag{64}$$

$\hat{a}^{\varepsilon}(\omega, \kappa_1, x_3) : \mathbb{R}^+ \times \mathbb{R}^+ \times \mathbb{R} \to \mathbb{R}$ and $\hat{b}^{\varepsilon}(\omega, \kappa_1, x_3) : \mathbb{R}^+ \times \mathbb{R}^+ \times \mathbb{R} \to \mathbb{R}$. The initial conditions are such that $\hat{a}^{\varepsilon}$ and $\hat{b}^{\varepsilon}$ are prescribed at $x_3 = 0$ and the radiation conditions demand

that $\hat{a}^\varepsilon$ and $\hat{b}^\varepsilon$ tend to zero as x_3 tends to $\pm\infty$. The random fluctuations are assumed to have the form $m(x_3) = g(Y(x_3))$, where Y is a homogeneous in x_3 Markov process with values in a compact space [40], and that this process is strongly ergodic and satisfies the Fredholm alternative [6], and the real bounded function g satisfies the centering condition $\mathbb{E}[g(Y(0))] = 0$. Equation (63) can be recast into an initial value problem using

$$\begin{bmatrix} \hat{a}^\varepsilon(x_3) \\ \hat{b}^\varepsilon(x_3) \end{bmatrix} = \mathbf{P}^\varepsilon(x_3) \begin{bmatrix} \hat{a}^\varepsilon(0) \\ \hat{b}^\varepsilon(0) \end{bmatrix}, \tag{65}$$

where the propagator matrix

$$\mathbf{P}^\varepsilon(x_3) = \begin{bmatrix} \chi_1^\varepsilon(x_3) & \chi_2^\varepsilon(x_3) \\ \chi_3^\varepsilon(x_3) & \chi_4^\varepsilon(x_3) \end{bmatrix}, \tag{66}$$

is formed from eigensolutions of Equation (63), and $\mathbf{P}^\varepsilon(x_3 = 0) = \mathbf{I}$. It follows that

$$\frac{\partial \mathbf{P}^\varepsilon}{\partial x_3} = \mathbf{H}^\varepsilon \mathbf{P}^\varepsilon. \tag{67}$$

3.3. Diffusion approximation theorem

We now apply a diffusion-approximation result of [40] to obtain a set of matrix-valued stochastic differential equations. From the definitions of δ_j then $\mathbf{H}^\varepsilon$ can be expanded as

$$\begin{aligned} \mathbf{H}^\varepsilon\left(\frac{x_3}{\varepsilon^2}, m\left(\frac{x_3}{\varepsilon^2}\right)\right) = {} & \frac{i}{\varepsilon} m\left(\frac{x_3}{\varepsilon^2}\right) \begin{bmatrix} \alpha\Gamma_\alpha & 0 \\ 0 & \alpha\Gamma_\alpha \end{bmatrix} \\ & - \frac{i}{2\varepsilon} m\left(\frac{x_3}{\varepsilon^2}\right) \phi\left(\Gamma_\beta + \Gamma_\gamma\right) \begin{bmatrix} 1 & 0 \\ 0 & -1 \end{bmatrix} \\ & + \frac{1}{2\varepsilon} m\left(\frac{x_3}{\varepsilon^2}\right) \phi\left(\Gamma_\beta - \Gamma_\gamma\right) \cos\left(\frac{2\phi x_3}{\varepsilon^2}\right) \begin{bmatrix} 0 & -i \\ i & 0 \end{bmatrix} \\ & + \frac{1}{2\varepsilon} m\left(\frac{x_3}{\varepsilon^2}\right) \phi\left(\Gamma_\beta - \Gamma_\gamma\right) \sin\left(\frac{2\phi x_3}{\varepsilon^2}\right) \begin{bmatrix} 0 & 1 \\ 1 & 0 \end{bmatrix}. \end{aligned} \tag{68}$$

Hence, Equation (66) can be written as

$$\frac{\mathrm{d}}{\mathrm{d}x_3}\mathbf{P}^\varepsilon(x_3) = \frac{1}{\varepsilon}\mathbf{F}\left(\mathbf{P}^\varepsilon(x_3), m\left(\frac{x_3}{\varepsilon^2}\right), \frac{x_3}{\varepsilon^2}\right) \tag{69}$$

$$= \frac{i}{\varepsilon} m\left(\frac{x_3}{\varepsilon^2}\right) \alpha\Gamma_\alpha \mathbf{I}\,\mathbf{P}^\varepsilon(x_3) \tag{70}$$

$$\begin{aligned} & - \frac{i}{2\varepsilon} m\left(\frac{x_3}{\varepsilon^2}\right) \phi\left(\Gamma_\beta + \Gamma_\gamma\right) \sigma_3 \mathbf{P}^\varepsilon(x_3) \\ & + \frac{1}{2\varepsilon} m\left(\frac{x_3}{\varepsilon^2}\right) \phi\left(\Gamma_\beta - \Gamma_\gamma\right) \cos\left(\frac{2\phi x_3}{\varepsilon^2}\right) \sigma_2 \mathbf{P}^\varepsilon(x_3) \\ & + \frac{1}{2\varepsilon} m\left(\frac{x_3}{\varepsilon^2}\right) \phi\left(\Gamma_\beta - \Gamma_\gamma\right) \sin\left(\frac{2\phi x_3}{\varepsilon^2}\right) \sigma_1 \mathbf{P}^\varepsilon(x_3), \end{aligned} \tag{71}$$

and $\boldsymbol{\sigma}_1, \boldsymbol{\sigma}_2, \boldsymbol{\sigma}_3$ are the Pauli spin matrices

$$\boldsymbol{\sigma}_1 = \begin{bmatrix} 0 & 1 \\ 1 & 0 \end{bmatrix}, \quad \boldsymbol{\sigma}_2 = \begin{bmatrix} 0 & -i \\ i & 0 \end{bmatrix}, \quad \boldsymbol{\sigma}_3 = \begin{bmatrix} 1 & 0 \\ 0 & -1 \end{bmatrix}. \tag{72}$$

The matrix $\mathbf{F}$ can be written as

$$\mathbf{F} = \sum_{p=1}^{4} g_p(m, \tau)\, \mathbf{h}_p \mathbf{P}^{\varepsilon}, \tag{73}$$

where $\tau = x_3/\varepsilon^2$,

$$\mathbf{h} = \begin{bmatrix} i\alpha\Gamma_\alpha \mathbf{I} \\ -\frac{i\phi(\Gamma_\beta + \Gamma_\gamma)}{2}\boldsymbol{\sigma}_3 \\ \frac{\phi(\Gamma_\beta - \Gamma_\gamma)}{2}\boldsymbol{\sigma}_2 \\ \frac{\phi(\Gamma_\beta - \Gamma_\gamma)}{2}\boldsymbol{\sigma}_1 \end{bmatrix} \quad \text{and} \quad \mathbf{g}(m, \tau) = \begin{bmatrix} m \\ m \\ m\cos(2\phi\tau) \\ m\sin(2\phi\tau) \end{bmatrix}. \tag{74}$$

From Equations (44), (47), (48) and (51) ϕ does not depend on frequency, and is instead a function of $\rho, c_3, \bar{\theta}, N$ and F. Equation (71) is also independent of frequency due to the scaling requirement that $\omega \sim \varepsilon^{-2}$ in the weakly heterogeneous regime. The correlation matrix $\mathbf{C} = (C_{pq})_{p,q=1,2,3,4}$ is computed using the covariance of the random process m. The correlation integrals can be assembled in a matrix, together with symmetric (S) and antisymmetric (AS) elements

$$\mathbf{C} = \begin{bmatrix} \Upsilon(0) & \Upsilon(0) & 0 & 0 \\ \Upsilon(0) & \Upsilon(0) & 0 & 0 \\ 0 & 0 & \frac{1}{2}\Upsilon(\phi) & \frac{1}{2}\Upsilon^{(AS)}(\phi) \\ 0 & 0 & -\frac{1}{2}\Upsilon^{(AS)}(\phi) & \frac{1}{2}\Upsilon(\phi) \end{bmatrix}, \tag{75}$$

$$\mathbf{C}^{(S)} = \begin{bmatrix} \Upsilon(0) & 0 & 0 & 0 \\ 0 & \Upsilon(0) & 0 & 0 \\ 0 & 0 & \frac{1}{2}\Upsilon(\phi) & 0 \\ 0 & 0 & 0 & \frac{1}{2}\Upsilon(\phi) \end{bmatrix}, \tag{76}$$

and

$$\mathbf{C}^{(AS)} = \begin{bmatrix} 0 & \Upsilon(0) & 0 & 0 \\ \Upsilon(0) & 0 & 0 & 0 \\ 0 & 0 & 0 & \frac{1}{2}\Upsilon^{(AS)}(\phi) \\ 0 & 0 & -\frac{1}{2}\Upsilon^{(AS)}(\phi) & 0 \end{bmatrix}, \tag{77}$$

where the correlation integrals are defined as

$$\Upsilon(\phi) = 2\int_0^\infty \mathbb{E}\left[m(0)m(x_3)\right]\cos(2\phi x_3)\, \mathrm{d}x_3, \tag{78}$$

and

$$\Upsilon^{(AS)}(\phi) = 2\int_0^\infty \mathbb{E}\left[m(0)m(x_3)\right]\sin(2\phi x_3)\, \mathrm{d}x_3. \tag{79}$$

The quantity $\Upsilon(\phi)$ is a non-negative real number, as it is proportional to the power spectral density of the stationary random process m. Details of how to compute the correlation integrals numerically for a given material are in [17]. Now the diffusion approximation theorem

([40], page 161) can be used to show that $\mathbf{P}^{\varepsilon}(x_3)$ converges in distribution to $\mathbf{P}(x_3)$ where $\mathbf{P}(x_3)$ is the solution of the Stratonovich stochastic differential equation

$$\begin{aligned}\mathrm{d}\mathbf{P} = {} & i\sqrt{\Upsilon(0)}\left(\alpha\Gamma_\alpha\mathbf{P}\circ\mathrm{d}W_1(x_3) - \frac{\phi}{2}(\Gamma_\beta+\Gamma_\gamma)\boldsymbol{\sigma}_3\mathbf{P}\circ\mathrm{d}W_2(x_3)\right)\\ & + \frac{\phi}{2\sqrt{2}}(\Gamma_\beta-\Gamma_\gamma)\sqrt{\Upsilon(\phi)}\,(\boldsymbol{\sigma}_2\mathbf{P}\circ\mathrm{d}W_3(x_3) + \boldsymbol{\sigma}_1\mathbf{P}\circ\mathrm{d}W_4(x_3))\\ & + \frac{1}{2}\left(\Upsilon(0)\alpha\Gamma_\alpha\phi(\Gamma_\beta+\Gamma_\gamma) + i\frac{\Upsilon^{AS}(\phi)}{4}\phi^2(\Gamma_\beta-\Gamma_\gamma)^2\right)\boldsymbol{\sigma}_3\mathbf{P}\,\mathrm{d}x_3. \end{aligned} \tag{80}$$

Using Equations (66) and (72) this can be written

$$\begin{aligned}\mathrm{d}\begin{bmatrix}\chi_1 & \chi_2\\ \chi_3 & \chi_4\end{bmatrix} = {} & iA_1\begin{bmatrix}\chi_1 & \chi_2\\ \chi_3 & \chi_4\end{bmatrix}\circ\mathrm{d}W_1 + iA_2\begin{bmatrix}\chi_1 & \chi_2\\ -\chi_3 & -\chi_4\end{bmatrix}\circ\mathrm{d}W_2 + iA_3\begin{bmatrix}-\chi_3 & -\chi_4\\ \chi_1 & \chi_2\end{bmatrix}\circ\mathrm{d}W_3\\ & + A_3\begin{bmatrix}\chi_3 & \chi_4\\ \chi_1 & \chi_2\end{bmatrix}\circ\mathrm{d}W_4 + (A_4+iA_5)\begin{bmatrix}\chi_1 & \chi_2\\ -\chi_3 & -\chi_4\end{bmatrix}\mathrm{d}x_3, \end{aligned} \tag{81}$$

where $A_1 = \alpha\Gamma_\alpha\sqrt{\Upsilon(0)}, A_2 = -(\phi(\Gamma_\beta+\Gamma_\gamma)/2)\sqrt{\Upsilon(0)}, A_3 = (\phi/(2\sqrt{2}))(\Gamma_\beta-\Gamma_\gamma)\sqrt{\Upsilon(\phi)}$, $A_4 = (1/2)\alpha\Gamma_\alpha\phi(\Gamma_\beta+\Gamma_\gamma)\Upsilon(0)$ and $A_5 = (1/8)\phi^2(\Gamma_\beta-\Gamma_\gamma)^2\Upsilon^{AS}(\phi)$.

Introducing the polar coordinate parameterization for the elements of the propagator matrix via $\chi_1(x_3) = a(x_3)\,\mathrm{e}^{ib(x_3)}$, $\chi_2(x_3) = g(x_3)\,\mathrm{e}^{ih(x_3)}$, $\chi_3(x_3) = j(x_3)\,\mathrm{e}^{ik(x_3)}$ and $\chi_4(x_3) = p(x_3)\,\mathrm{e}^{iq(x_3)}$, the equations for the radial and phase parts of the propagator functions can be written in matrix form as

$$\begin{aligned} d\begin{bmatrix}a\\ b\\ g\\ h\\ j\\ k\\ p\\ q\end{bmatrix} = {} & \begin{bmatrix} 0 & 0 & A_3 j\sin(k-b) & A_3 j\cos(k-b)\\ A_1 & A_2 & -A_3(j/a)\cos(k-b) & A_3(j/a)\sin(k-b)\\ 0 & 0 & A_3 p\sin(q-h) & A_3 p\cos(q-h)\\ A_1 & A_2 & -A_3(p/g)\cos(q-h) & A_3(p/g)\sin(q-h)\\ 0 & 0 & -A_3 a\sin(b-k) & A_3 a\cos(b-k)\\ A_1 & -A_2 & A_3(a/j)\cos(b-k) & A_3(a/j)\sin(b-k)\\ 0 & 0 & -A_3 g\sin(h-q) & A_3 g\cos(h-q)\\ A_1 & -A_2 & A_3(g/p)\cos(h-q) & A_3(g/p)\sin(h-q)\end{bmatrix}\circ d\begin{bmatrix}xW_1\\ W_2\\ W_3\\ W_4\end{bmatrix}\\ & + \begin{bmatrix}A_4 a\\ A_5\\ A_4 g\\ A_5\\ -A_4 j\\ -A_5\\ -A_4 p\\ -A_5\end{bmatrix}\mathrm{d}x_3. \end{aligned} \tag{82}$$

Using Jacobi's formula and Equation (67) gives

$$\frac{\mathrm{d}\det\{\mathbf{P}^{\varepsilon}\}}{\mathrm{d}x_3} = \mathrm{Tr}\left(\mathbf{H}^{\varepsilon}\right)\det\left\{\mathbf{P}^{\varepsilon}\right\}, \tag{83}$$

which together with Equation (64) gives $\mathrm{Tr}(\mathbf{H}^{\varepsilon}) = 2i\alpha\Gamma_{\alpha} m(x_3/\varepsilon^2)$. Solving this differential equation yields

$$\det\{\mathbf{P}^{\varepsilon}\} = \exp\left(2i\alpha\Gamma_{\alpha}\int_0^{x_3/\varepsilon^2} m(s)\,\mathrm{d}s\right), \tag{84}$$

and hence $|\det\{\mathbf{P}^{\varepsilon}(x_3)\}| = 1$, and so Equation (66) implies

$$|\chi_1\chi_4 - \chi_2\chi_3| = 1. \tag{85}$$

This conservation of energy relationship can be written as

$$\cos(b+q-h-k) = \frac{a^2p^2 + g^2j^2 - 1}{2apgj} = D_1(a,g,j,p), \tag{86}$$

and so $q-h = \cos^{-1}(D_1) + (k-b)$, which gives $\cos(q-h) = D_1\cos(k-b) - \sqrt{1-D_1^2}\sin(k-b)$ and $\sin(h-q) = \sqrt{1-D_1^2}\cos(k-b) + D_1\sin(k-b)$. Equation (82) contains the Stratonovich subsystem

$$d\begin{bmatrix} g \\ h \\ p \\ q \end{bmatrix} = \begin{bmatrix} 0 & 0 & A_3 p\sin(q-h) & A_3 p\cos(q-h) \\ A_1 & A_2 & -A_3\frac{p}{g}\cos(q-h) & A_3\frac{p}{g}\sin(q-h) \\ 0 & 0 & A_3 g\sin(q-h) & A_3 g\cos(q-h) \\ A_1 & -A_2 & A_3\frac{g}{p}\cos(q-h) & -A_3\frac{g}{p}\sin(q-h) \end{bmatrix} \circ d\begin{bmatrix} W_1 \\ W_2 \\ W_3 \\ W_4 \end{bmatrix} + \begin{bmatrix} A_4 g \\ A_5 \\ -A_4 p \\ -A_5 \end{bmatrix} \mathrm{d}x_3, \tag{87}$$

which in Itô form reads

$$\begin{aligned} d\begin{bmatrix} g \\ h \\ p \\ q \end{bmatrix} &= \begin{bmatrix} 0 & 0 & A_3 p\sin(q-h) & A_3 p\cos(q-h) \\ A_1 & A_2 & -A_3\frac{p}{g}\cos(q-h) & A_3\frac{p}{g}\sin(q-h) \\ 0 & 0 & A_3 g\sin(q-h) & A_3 g\cos(q-h) \\ A_1 & -A_2 & A_3\frac{g}{p}\cos(q-h) & -A_3\frac{g}{p}\sin(q-h) \end{bmatrix} d\begin{bmatrix} W_1 \\ W_2 \\ W_3 \\ W_4 \end{bmatrix} \\ &\quad + \begin{bmatrix} A_4 g + \frac{A_3^2}{2}\left(\frac{p^2}{g} + 2g\right) \\ A_5 \\ -A_4 p + \frac{A_3^2}{2}\left(2p + \frac{g^2}{p}\right) \\ -A_5 \end{bmatrix} \mathrm{d}x_3. \end{aligned} \tag{88}$$

Now introduce the orthogonal Itô transform to separate this system

$$\begin{bmatrix} W_3^{\star} \\ W_4^{\star} \end{bmatrix} = \int_0^{x_3} \begin{bmatrix} D_2^s & D_2^c \\ -D_2^c & D_2^s \end{bmatrix} d\begin{bmatrix} W_3 \\ W_4 \end{bmatrix}, \tag{89}$$

and using Equation (86) gives

$$D_2^s = -\sqrt{1-D_1^2}\cos(k-b) - D_1\sin(k-b) = \sin(q-h), \tag{90}$$

and

$$D_2^c = D_1\cos(k-b) - \sqrt{1-D_1^2}\sin(k-b) = \cos(q-h). \tag{91}$$

Note that

$$(D_2^s)^2 + (D_2^c)^2 = 1, \quad \text{and} \quad \left[D_2^s, D_2^c\right].\left[-D_2^c, D_2^s\right] = 0, \tag{92}$$

which ensures the transform is orthogonal. Furthermore, one can show that the transform is justified [45] by showing that the correlation is zero, and the variance of D_2^s and D_2^c is zero. So the system of Itô SDE's (88) can be rewritten as

$$d\begin{bmatrix} g \\ h \\ p \\ q \end{bmatrix} = \begin{bmatrix} 0 & 0 & A_3 p & 0 \\ A_1 & A_2 & 0 & A_3 \frac{p}{g} \\ 0 & 0 & A_3 g & 0 \\ A_1 & -A_2 & 0 & -A_3 \frac{g}{p} \end{bmatrix} d\begin{bmatrix} W_1 \\ W_2 \\ W_3^\star \\ W_4^\star \end{bmatrix} + \begin{bmatrix} A_4 g + \frac{A_3^2}{2}\left(\frac{p^2}{g} + 2g\right) \\ A_5 \\ -A_4 p + \frac{A_3^2}{2}\left(2p + \frac{g^2}{p}\right) \\ -A_5 \end{bmatrix} \mathrm{d}x_3. \tag{93}$$

3.4. Moments of the power transmission coefficient

There is an incident unit pulse impinging the slab of layered random media from the left at $x_3 = 0$ with a radiation condition in the homogeneous half-space $x_3 \in (0, \infty)$. The mode amplitudes governed by Equations (55) and (56) satisfy the boundary conditions

$$\hat{a}^\varepsilon(0) = 1, \quad \hat{b}^\varepsilon(L) = 0. \tag{94}$$

The linear system (65) then gives

$$\begin{bmatrix} \hat{a}^\varepsilon(L) \\ 0 \end{bmatrix} = \begin{bmatrix} \chi_1^\varepsilon(L) & \chi_2^\varepsilon(L) \\ \chi_3^\varepsilon(L) & \chi_4^\varepsilon(L) \end{bmatrix} \begin{bmatrix} 1 \\ \hat{b}^\varepsilon(0) \end{bmatrix}, \tag{95}$$

and the reflection and transmission coefficients can then be written as

$$R_\omega^\varepsilon(L) = \hat{b}^\varepsilon(\omega, 0), \quad \text{and} \quad T_\omega^\varepsilon(L) = \hat{a}^\varepsilon(L), \tag{96}$$

and so

$$R_\omega^\varepsilon(L) = -\frac{\chi_3^\varepsilon(L)}{\chi_4^\varepsilon(L)}, \quad T_\omega^\varepsilon(L) = \frac{\chi_1^\varepsilon(L)\chi_4^\varepsilon(L) - \chi_2^\varepsilon(L)\chi_3^\varepsilon(L)}{\chi_4^\varepsilon(L)}. \tag{97}$$

The transmission coefficient $T_\omega^\varepsilon(L)$ converges in distribution (as $\varepsilon \to 0$) to $T_\omega(L)$ and the power transmission coefficient ($\tau_\omega(L)$ say) is then given by

$$\tau_\omega(L) = |T_\omega(L)|^2 = |\chi_4(L)|^{-2} = \frac{1}{p^2}, \tag{98}$$

where the conservation of energy relation (85) has been used. Note that the initial condition of the power transmission coefficient $\tau_\omega(L = 0) = 1$ follows from that fact that $\mathbf{P}(x_3 = 0) = \mathbf{I}$. The moments of the power transmission coefficient can then be calculated via

$$\mathbb{E}[(\tau_\omega(L))^n] = \int_1^{p_\infty} \int_0^{g_\infty} \frac{P(L, g, p)}{p^{2n}} \, \mathrm{d}g \, \mathrm{d}p, \tag{99}$$

where $P(L, g, p)$ is the probability density function associated with p at $x_3 = L$. From Equation (93) it is clear that (dg, dp) and (dh, dq) decouple into two independent subsystems. Studying the statistics of the power transmission coefficient requires solving the

(dg, dp) system

$$d\begin{bmatrix} g \\ p \end{bmatrix} = \begin{bmatrix} A_3 p & 0 \\ A_3 g & 0 \end{bmatrix} d\begin{bmatrix} W_3^\star \\ W_4^\star \end{bmatrix} + \begin{bmatrix} A_4 g + \frac{A_3^2}{2}\left(\frac{p^2}{g} + 2g\right) \\ -A_4 p + \frac{A_3^2}{2}\left(2p + \frac{g^2}{p}\right) \end{bmatrix} \mathrm{d}x_3. \tag{100}$$

The infinitesimal generator $\mathcal{L}_{g,p}$ is then

$$\mathcal{L}_{g,p} = \frac{1}{2}\left(A_3^2 p^2 \frac{\partial^2}{\partial g^2} + 2A_3^2 pg \frac{\partial^2}{\partial g \partial p} + A_3^2 g^2 \frac{\partial^2}{\partial p^2}\right) + \left(A_4 g + \frac{A_3^2}{2}\left(\frac{p^2}{g} + 2g\right)\right)\frac{\partial}{\partial g} + \left(\frac{A_3^2}{2}\left(2p + \frac{g^2}{p}\right) - A_4 p\right)\frac{\partial}{\partial p}. \tag{101}$$

Using the substitution

$$\mathcal{G} = g^2, \tag{102}$$

gives

$$\mathcal{L}_{\mathcal{G},p} = 2A_3^2 p^2 \mathcal{G}\frac{\partial^2}{\partial \mathcal{G}^2} + \left(2A_3^2 p^2 + \mathcal{G}(2A_4 + 2A_3^2)\right)\frac{\partial}{\partial \mathcal{G}} + 2A_3^2 p\mathcal{G}\frac{\partial^2}{\partial \mathcal{G}\partial p} + \frac{A_3^2}{2}\mathcal{G}\frac{\partial^2}{\partial p^2} + \left(\frac{A_3^2}{2}\left(2p + \frac{\mathcal{G}}{p}\right) - A_4 p\right)\frac{\partial}{\partial p}. \tag{103}$$

The adjoint of Equation (103) is

$$\mathcal{L}^\star_{\mathcal{G},p} = 2A_3^2 p^2 \mathcal{G}\frac{\partial^2}{\partial \mathcal{G}^2} + \left(2A_3^2 p^2 - 2\mathcal{G}A_4\right)\frac{\partial}{\partial \mathcal{G}} + \left(2A_3^2 p - \frac{A_3^2}{2}\left(2p + \frac{\mathcal{G}}{p}\right) + A_4 p\right)\frac{\partial}{\partial p} + 2A_3^2 \mathcal{G} p\frac{\partial^2}{\partial \mathcal{G}\partial p} + \frac{A_3^2}{2}\mathcal{G}\frac{\partial^2}{\partial p^2} + \left(\frac{A_3^2 \mathcal{G}}{2p^2} + 3A_3^2 + 3A_4\right) I_d. \tag{104}$$

The Fokker–Planck equation for the pair of processes ($\mathcal{G}$, p) is then

$$\frac{\partial P}{\partial L}(L, \mathcal{G}, p) = \mathcal{L}^\star_{\mathcal{G},p} P(L, \mathcal{G}, p), \quad P(L = 0, \mathcal{G}, p) = \delta(\mathcal{G})\delta(p - 1). \tag{105}$$

By defining the following

$$\mathbf{a}^\star = \begin{bmatrix} 2A_3^2 p^2 \mathcal{G} & A_3^2 \mathcal{G} p \\ A_3^2 \mathcal{G} p & \frac{A_3^2}{2}\mathcal{G} \end{bmatrix}, \quad \mathbf{b}^\star = \begin{bmatrix} 2A_3^2 p^2 - 2\mathcal{G}A_4 \\ 2A_3^2 p - A_3^2(2p + \mathcal{G}/p)/2 + A_4 p \end{bmatrix}, \quad \nabla = \begin{bmatrix} \partial/\partial \mathcal{G} \\ \partial/\partial p \end{bmatrix}, \tag{106}$$

and $Q = A_3^2 \mathcal{G}/(2p^2) + 3A_3^2 + 3A_4$, the Fokker–Planck Equation (105) can be rewritten as

$$\frac{\partial P}{\partial L}(L, \mathcal{G}, p) = (\mathbf{a}^\star \nabla + \mathbf{b}^\star) \cdot \nabla P(L, \mathcal{G}, p) + QP(L, \mathcal{G}, p). \tag{107}$$

Equation (107) can be rewritten by using the identity $(\mathbf{a}^\star\nabla + \mathbf{b}^\star)\cdot\nabla = \nabla\cdot(\mathbf{a}^\star\nabla) + \mathbf{c}^\star\cdot\nabla$, where

$$\mathbf{c}^\star = \mathbf{b}^\star - \nabla^T\mathbf{a} = \begin{bmatrix} -A_3^2\mathcal{G} - 2\mathcal{G}A_4 \\ A_3^2 p - A_3^2(2p + \mathcal{G}/p)/2 + A_4 p \end{bmatrix}. \tag{108}$$

The Fokker–Planck equation may then be written as

$$\frac{\partial P}{\partial L}(L,\mathcal{G},p) = \nabla\cdot\mathbf{a}^\star\nabla P(L,\mathcal{G},p) + \mathbf{c}^\star\cdot\nabla P(L,\mathcal{G},p) + QP(L,\mathcal{G},p), \tag{109}$$

with Dirac delta initial condition

$$P(L=0,\mathcal{G},p) = \delta(\mathcal{G})\delta(p-1). \tag{110}$$

The Fokker–Planck Equation (109) is then expressed in its weak form to obtain a numerical solution for the probability density function $P(L,\mathcal{G},p)$. A numerical solution is obtained using the FeniCS package [44] in Python. With Neumann boundary conditions and test function $v(\mathbf{x})$ ($\mathbf{x} = (\mathcal{G},p)$, $\Omega = [0,1]\times[1,\infty]$) the weak form of the problem is

$$a(P,v) = L(v), \tag{111}$$

where

$$a(P,v) = \int_\Omega \left(v(\mathbf{x})P + \Delta L\, S(P)\right)\mathrm{d}\mathbf{x}, \tag{112}$$

$$L(v) = \int_\Omega v(\mathbf{x})P\,\mathrm{d}\mathbf{x}, \tag{113}$$

with $S(P) = \nabla v(\mathbf{x})\cdot\mathbf{a}^\star\nabla P - v(\mathbf{x})\mathbf{c}^\star\cdot\nabla P - v(\mathbf{x})QP$. A rectangular mesh is used for the domain Ω and a convergence study for optimal mesh discretization suggests a coarse mesh in the $\mathcal{G}$ direction and a very fine mesh in the p direction is required.

4. Numerical results

The properties of austenitic steel (see Table 1) were used to obtain the diffusion coefficients (given below Equation (81)) which appear in the Fokker–Planck Equation (111). Austenitic steel was chosen as it is an anisotropic heterogeneous layered engineering material. of a The numerical solution of this equation provides the probability density function $P(L,\mathcal{G},p)$ which is then used to compute the statistical moments of the power transmission coefficients in Equation (99). A frequency ($\tilde{\omega}\sim\varepsilon^{-2}$) and a mean wave speed of $c_3 = 4500\,\mathrm{ms}^{-1}$ were used together with the stiffness tensor constants in Table 1. The correlation integral $\Upsilon(\phi)$ in Equation (78) is set to 1 for the following simulations, however this can be calculated for a specific material as outlined in [17].

In Figure 3 the mean power transmission coefficient versus the depth into the random medium L is plotted. The power transmission coefficient gives the amount of energy that is sent through the medium, decreasing as a function of the length L of the medium. As the degree of anisotropy ν is increased, an increased decay in the amplitude of the coherent wave is observed.

Figure 3 also shows the variance in the power transmission coefficient.

Table 1. Table of material constants for austenitic steel [18].

	Elastic material constants and density					
	$\bar{\bar{c}}_{11}$	$\bar{\bar{c}}_{33}$	$\bar{\bar{c}}_{44}$	$\bar{\bar{c}}_{66}$	$\bar{\bar{c}}_{13}$	ρ
Austenitic steel	217.1 GPa	263.2 GPa	82.4 GPa	128.4 GPa	144.4 GPa	8100 kgm^{-3}

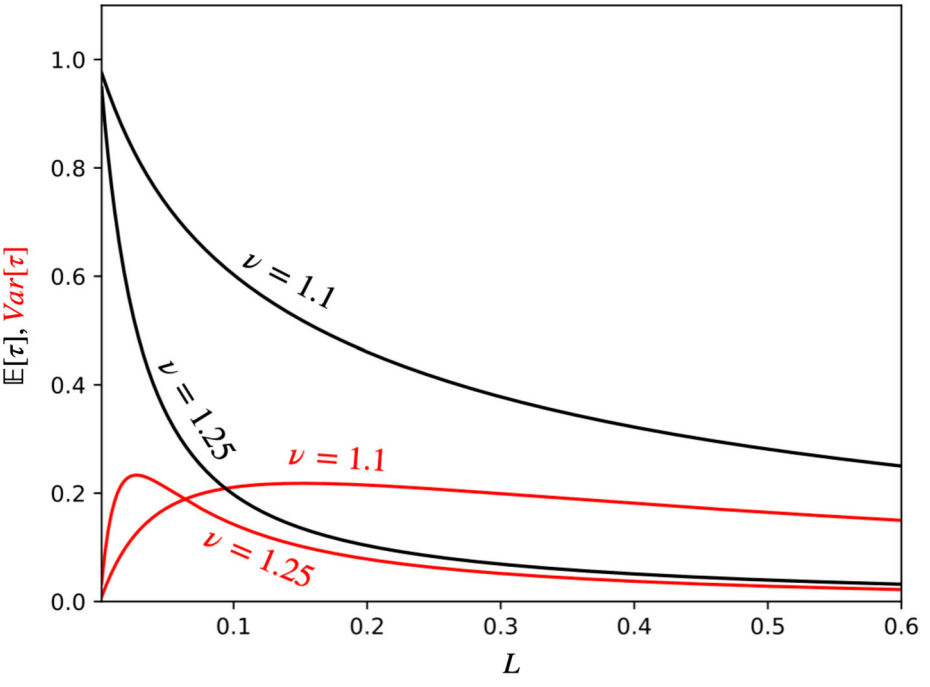

Figure 3. Plots of the mean transmission coefficient (see Equation (99)) (black) with the associated variance (red) for the degree of anisotropy $\nu = (1.1,\ 1.25)$ versus L; the non-dimensionalized penetration depth. The material parameters are given in Tables 1 and 2. Eventually the variance will asymptote to zero, and at that stage the process has self averaged. This means that very thick materials will have a narrow probability density function and so the mean can be used to characterize the material. Therefore, homogenization could be applied in such cases, however, in intermediate material thicknesses, a stochastic approach such as that contained in this paper is needed. See the appendix for constants used in the simulation.

For an infinitesimally thin material (characterized by $L = 0$) the energy of the wave is fully transmitted ($\mathbb{E}[\tau] = 1$) with no uncertainty and therefore the red curve in Figure 3 starts at the origin. As the thickness increases, then the mean transmission coefficient decreases. This is more marked for materials with a higher degree of anisotropy. At the same time the uncertainty increases and peaks at a depth of material that varies with the degree of anisotropy. It can be seen that this high uncertainty persists for a large range of lengths L for $\nu = 1.1$. Solving for the power transmission through the finite element method necessitates investigating element sizes for convergence whilst minimizing computational complexity and the associated computational expense. By conducting a methodical search across this hyper-parameter space (element and domain size), we identified the most efficient solver settings that struck a balance between accuracy and computational time. We

Table 2. Material constants used in numerical simulations.

Parameter	Value	Units
c_3	4500	LT^{-1}
ρ	8100	ML^{-3}
$\bar{c}_{66}$	8.914×10^{10}	$ML^{-1}T^{-2}$
$\bar{c}_{44}$	1.217×10^{11}	$ML^{-1}T^{-2}$
$\bar{c}_{64}$	-1.626×10^{10}	$ML^{-1}T^{-2}$
$\tilde{\alpha}$	-1.671×10^{-1}	[–]
$\tilde{\beta}$	-1.348	[-]
$\tilde{\gamma}$	-1.716×10^{-1}	[–]
Γ_α	-2.267	[-]
Γ_β	-2.674×10^{-1}	[–]
Γ_γ	1.291	[–]
A_1	8.472×10^{-1}	[–]
A_2	-5.503×10^{-1}	[–]
A_3	-5.924×10^{-1}	[–]
A_4	4.662×10^{-1}	[–]
A_5	3.510×10^{-1}	[–]
$\tilde{L}$	1.425	[–]

employed the initial condition (110) in our hyperparameter search, ensuring the conservation of probability as we increased the length of the medium (L). Our findings revealed that utilizing a box mesh with spatial dimensions $(x, y, z)_{\text{initial}} = (1 \times 10^{-4}, 1 \times 10^{-4}, 1)$ to $(x, y, z)_{\text{final}} = (4, 4, 4)$ and a density of 1000 elements in each axis yielded promising results without incurring significant computational costs. The mesh resolution is governed by the number of cells in each direction (n_x, n_y, n_z).

5. Concluding remarks

A probabilistic model of a monochromatic, horizontally polarized shear wave propagating in a randomly layered heterogeneous medium constructed of locally anisotropic layers has been constructed and studied. The spatial scaling regime is such that the internal microstructure of the medium interacts with the probing wave to produce an incoherent coda wave. The orientation of the anisotropic material varies randomly from layer to layer according to a Markov process. Using elastodynamic equations, expressions for the forward and backward wave-modes, which describe the reflected and transmitted energy for the input wave were derived. Via a series of transformations, a system of stochastic differential equations was then derived for a propagator formulation of this wave-mode problem. Utilizing a limit theorem from stochastic analysis a linear partial differential equation (Fokker–Planck equation) for the probability density function associated with the transmitted power was derived which was solved via a finite element package in Python. Its numerical solution enabled an investigation into the effect that the material parameters have on the decay of energy in the coherent part of the transmitted probing wave.

In particular the mean and variance of the transmitted energy through a class of austenitic steel welds was calculated without the need for expensive Monte Carlo simulations. Varying the degree of anisotropy parameter ν had a significant impact on the attenuation of the coherent energy. It also shows when a homogenization approach would be valid (small higher moments in the probability density function) for a given material, mean layer size and wavelength. By capturing the randomness present in materials such

as austenitic welds, this model could be used by experimental scientists in the NDT community; calculations of the correlation integrals can be obtained from experimental images of the material microstructure [17]. For example, this model could estimate optimal frequency ranges for a probing ultrasonic wave in order to image (with good resolution) to a certain depth in a given random media. It could also be used in finite element simulations of ultrasonic wave propagation, to generate attenuation factors (and uncertainty quantification) for elastic wave propagation in such layered materials without the need for explicitly including the layer geometry in the simulation.

The probabilistic model presented in this paper could be used by experimentalists who are interested in developing techniques for the quality assurance of layered metallic components such as those found in additively manufactured or welded components. The model can assist in the choice of frequency content in the (source) laser generated ultrasound waves to ensure the maximum information on the underlying material microstructure is then contained in the transmitted wave; that is, when there is the maximum variance in the population of transmission coefficients (see Figure 3). This would provide the optimal environment for the tomographic reconstruction of the microstructure in the component's interior to be reconstructed.

Future work could include some experimental testing of the work in this paper. Metallic components (that are polycrystalline and anisotropic such as the Titanium alloy Ti-64 [16]) could be additively manufactured and a short pulsed laser then used to generate a time-domain, broadband ultrasonic wavefield that propagates through the material. A spatial array of detection lasers, distributed across the component's rear surface, could then record these transmitted ultrasonic waves using laser interferometry. Each of these transmitted waves will have a slightly different form and the variation in the transmission coefficient could be calculated for example. By then reducing the thickness of the component, by say milling, and repeating these measurements the effect of the component thickness (L) on the variation in the transmission coefficient could be calculated; this could create an experimental means of testing the results in Figure 3. This paper does not consider the full elastodynamic equations and longitudinal waves and the associated mode conversion or non-layered materials. Introducing these phenomena would introduce significant complexity and make analytical headway extremely difficult, therefore we consider this as a future extension of our work.

Disclosure statement

No potential conflict of interest was reported by the author(s).

Funding

This work was supported by a Ph.D. studentship from the National Physical Laboratory (NPL) and the University of Strathclyde. The authors would like to acknowledge the support of the research grant UKRI/EPSRC grant EP/P005268/2.

References

[1] Abrahams ID, Wickham GR. The propagation of elastic waves in a certain class of inhomogeneous anisotropic materials. I. The refraction of a horizontally polarized shear wave source. Proc R Soc London A. 1992;436:439–478.

[2] Brooks JA, Thompson A. Microstructural development and solidification cracking susceptibility of austenitic stainless steel welds. Int Mater Rev. 1991;36:16–44. doi: 10.1179/imr.1991.36.1.16
[3] Tant KMM, Galetti E, Mulholland AJ, et al. A transdimensional Bayesian approach to ultrasonic travel-time tomography for non- destructive testing. Inverse Probl. 2018;34:Article ID 095002. doi: 10.1088/1361-6420/aaca8f
[4] Zhang Y, Brady M, Smith SM. Segmentation of brain mr images through a hidden Markov random field model and the expectation-maximization algorithm. IEEE Trans Med Imaging. 2001;20:45–57. doi: 10.1109/42.906424
[5] Lewandowski JJ, Seifi M. Metal additive manufacturing: a review of mechanical properties. Annu Rev Mater Res. 2016;46:151–186. doi: 10.1146/matsci.2016.46.issue-1
[6] Garnier J, Sølna K. Apparent attenuation of shear waves propagating through a randomly anisotropic medium. Stoch Dyn. 2015;16(4):Article ID 1650009. doi: 10.1142/S02194937165 0009X
[7] Li C, Pain D, Wilcox PD, et al. Imaging composite material using ultrasonic arrays. NDT E Int. 2013;53:8–17. doi: 10.1016/j.ndteint.2012.07.006
[8] Gillespie DT. Exact stochastic simulation of coupled chemical reactions. J Phys Chem. 1977;81(25):2340–2361. doi: 10.1021/j100540a008
[9] Meyn SP, Tweedie RL. Markov chains and stochastic stability. 1993. (Communications and control engineering series).
[10] Higham DJ. An algorithmic introduction to numerical simulation of stochastic differential equations. SIAM Rev. 2001;43:525–546. doi: 10.1137/S0036144500378302
[11] Parnell WJ, Abrahams ID. Dynamic homogenization in periodic fibre reinforced media. quasi-static limit for sh waves. Wave Motion. 2006;43:474–498. doi: 10.1016/j.wavemoti.2006.03.003
[12] Verna E, Genta G, Galetto M, et al. Economic impact of quality inspection in manufacturing: a proposal for a novel cost modeling. In: Proceedings of the institution of mechanical engineers, part B: journal of engineering manufacture. Vol. 236; 2022. p. 1508–1517.
[13] Pant M, Nagdeve L, Kumar H, et al. A contemporary investigation of metal additive manufacturing techniques. Sadhana. 2022;47:1–19. doi: 10.1007/s12046-021-01770-6
[14] Lin X, Zhu K, Fuh JYH, et al. Metal-based additive manufacturing condition monitoring methods: from measurement to control. ISA Trans. 2021;120:147–166. doi: 10.1016/j.isatra.2021.03.001
[15] Davis G, Stratoudaki T, Lukacs P, et al. Near-surface defect detection in additively manufactured components using laser induced phased arrays with surface acoustic wave crosstalk suppression. Mater Des. 2023;236:Article ID 112453. doi: 10.1016/j.matdes.2023.112453
[16] Kasemer M, Echlin MP, Stinville JC, et al. On slip initiation in equiaxed α/β ti-6al-4v. Acta Mater. 2017;136:288–302. doi: 10.1016/j.actamat.2017.06.059
[17] Ferguson AS, Tant KMM, Mulholland AJ. Modelling of ultrasonic waves in layered elastic heterogeneous materials. In: 2021 IEEE International Ultrasonics Symposium (IUS); Xi'an, China; 2021. p. 1–4.
[18] Spies M. Elastic waves in homogeneous and layered transversely isotropic media: plane waves and Gaussian wave packets. A general approach. J Acoust Soc Am. 1994;95:1748–1760. doi: 10.1121/1.408694
[19] Anderson D. Elastic wave propagation in layered anisotropic media. J Geophys Res. 1961;66:2953–2963. doi: 10.1029/JZ066i009p02953
[20] Pan E. Green's functions for geophysics: a review. Rep Prog Phys. 2019;82(10):Article ID 106801. doi: 10.1088/1361-6633/ab1877
[21] Humeida Y, Pinfield V, Challis R, et al. Simulation of ultrasonic array imaging of composite materials with defects. IEEE Trans Ultrason Ferroelectr Freq Control. 2013;60(9):1935–1948. doi: 10.1109/TUFFC.2013.2778
[22] Rokhlin SI, Wang L. Stable recursive algorithm for elastic wave propagation in layered anisotropic media: stiffness matrix method. J Acoust Soc Am. 2002;112(3):822–834. doi: 10.1121/1.149 7365
[23] Skelton EA, James J. Acoustics of anisotropic planar layered media. JSV. 1992;152(1):157–174. doi: 10.1016/0022-460X(92)90072-6

[24] Rokhlin SI, Wang L. Ultrasonic waves in layered anisotropic media: characterisation of multidirectional composites. Int J Solids Struct. 2002;39(21):5529–5545. doi: 10.1016/S0020-7683(02)00500-0
[25] Zhang Y, Gao Q. Stability analysis of the mixed variable method and its application in wave reflection and transmission in multilayered anisotropic structures. Arch Appl Mech. 2020;90:127–146. doi: 10.1007/s00419-019-01601-5
[26] Hosten B, Castaings M. Surface impedance matrices to model the propagation in multilayered media. Ultrasonics. 2003;41:501–507. doi: 10.1016/S0041-624X(03)00167-7
[27] Huang C, Nutt S. Sound transmission prediction by 3-d elasticity theory. Appl Acoust. 2009;70:730–736. doi: 10.1016/j.apacoust.2008.09.003
[28] Sun C, Li S. Three-dimensional effective elastic constants for thick laminates. J Compos Mater. 1988;22:629–639. doi: 10.1177/002199838802200703
[29] Liu M, Xiao H, Hu Q, et al. Floquet wave theory-based time-corrected ultrasonic total focusing method for fiber-reinforced composite laminate. Ultrasonics. 2021;116:Article ID 106467.
[30] Kausel E. Generalized stiffness matrix method for layered soils. Soil Dyn Earthq Eng. 2018;115:663–672. doi: 10.1016/j.soildyn.2018.09.003
[31] Chen L. Green's function for a transversely isotropic multi-layered half-space: an application of the precise integration method. Acta Mech. 2015;226:3881–3904. doi: 10.1007/s00707-015-1435-y
[32] Chen L. Three-dimensional Green's function for an anisotropic multi-layered half-space. Comput Mech. 2015;56:795–814. doi: 10.1007/s00466-015-1203-9
[33] Dahmen S, Ben Amor M, Ben Ghozlen M. Investigation of the coupled lamb waves propagation in viscoelastic and anisotropic multilayer composites by legendre polynomial method. Compos Struct. 2016;153:557–568. doi: 10.1016/j.compstruct.2016.06.068
[34] Dobson J, Tweedie A, Harvey G, et al. Finite element analysis simulations for ultrasonic array nde inspections. In: Proceedings of the AIP Conference. Vol. 1706; Minneapolis (MN), USA; 2015. p. 040005.
[35] Anand D, Groves R, Benedictus R. Modeling and imaging of ultrasonic array inspection of side drilled holes in layered anisotropic media. Sensors. 2021;12:4640. doi: 10.3390/s21144640
[36] Lu Y, Achenbach J. Effects of random deviations in interface properties on the propagation of ultrasound in thick composites. J Acoust Soc Am. 1991;90(5):2576–2585. doi: 10.1121/1.402061
[37] Yan DJ, Chen AL, Wang YS, et al. In-plane elastic wave propagation in nanoscale periodic layered piezoelectric structures. Int J Mech Sci. 2018;142:276–288. doi: 10.1016/j.ijmecsci.2018.04.054
[38] Orr LA, Mulholland AJ, O'Leary R, et al. Analysis of ultrasonic transducers with fractal architecture. Fractals. 2008;16(3):333–349. doi: 10.1142/S0218348X08004101
[39] Arguelles AP, Turner JA. Ultrasonic attenuation of polycrystalline materials with a distribution of grain sizes. J Acoust Soc Am. 2017;141(6):4347–4353. doi: 10.1121/1.4984290
[40] Fouque JP, Garnier J, Papanicolaou G, et al. Wave propagation and time reversal in randomly layered media. New York: Springer; 2007.
[41] Ferguson A, Mulholland AJ, Tant KMM, et al. Ultrasonic wave propagation in randomly layered heterogeneous media (In press). Wave Motion. 2022;120:Article ID 103138.
[42] Harvey G, Tweedie A, Carpentier C, et al. Finite element analysis of ultrasonic phased array inspections on anisotropic welds. In: AIP Conference Proceedings. Vol. 1335; San Diego, California; 2010. p. 827–834.
[43] Carpentier C, Nageswaran C, Tse YY. Microstructural quantification, modelling and array ultrasonics to improve the inspection of austenitic welds. Insight: Non-Destr Test Cond Monit. 2009;51(12):660–666. doi: 10.1784/insi.2009.51.12.660
[44] Alnæs MS, Blechta J, Hake J, et al. The fenics project version 1.5. Archive of Numerical Software. 2015;3(100):9–23.
[45] Bass RF. Stochastic processes. Cambridge University Press; 2011. (Cambridge series in statistical and probabilistic mathematics).